

# Probabilistic tractography, Path Integrals and the Fokker Planck equation

Marco Reisert

Dept. of Radiology, Medical Physics, University Hospital Freiburg, Germany

**Abstract**—Probabilistic tractography based on diffusion weighted MRI has become a powerful approach for quantifying structural brain connectivities. In several works the similarity of probabilistic tractography and path integrals was already pointed out. This work investigates this connection more closely. For the so called Wiener process, a Gaussian random walker, the equivalence is worked out. We identify the source of the asymmetry of usual random walkers approaches and show that there is a proper symmetrization, which leads to a new symmetric connectivity measure. To compute this measure we will use the Fokker-Planck equation, which is an equivalent representation of a Wiener process in terms of a partial differential equation. In experiments we show that the proposed approach leads a symmetric and robust connectivity measure.

## I. INTRODUCTION

Diffusion MRI has become a very important tool for understanding the living brain tissue ([16]). It can reveal both macro- and microstructural features of the neuronal network of the human brain. Tractography tries to characterize the structural connectome to understand the details of the interregional relationships of the human brain. Tractography algorithms may be divided in deterministic, streamline-based methods ([21], [2]), probabilistic approaches ([13], [22]) and global approaches ([19], [24]). In probabilistic tractography one basically draws samples from a distribution over paths and computes some statistics over these paths, for example, recording their endpoints. In some work the similarity to the notion of path integrals appearing in quantum mechanics [8] and statistical physics [18] was already pointed out [29], [5], [9], [4]. Rigorous mathematical investigations show that the basic stochastic process behind path integrals is a so called Wiener process, a continuous Gaussian random walker [31]. In this work we will recap the foundations of the theory of Wiener processes and path integrals. Based on this we build a path integral that leads to a symmetric brain connectivity measure. We will see that the source of asymmetry of conventional walker principles is due to particle conservation. By dropping particle conservation and starting from the path integral perspective we will find a symmetric brain connectivity measure. Besides the walker perspective and path integrals, there is a third, equivalent approach, which describes expectation values of Wiener walkers by partial differential equations (PDE). This equivalence will be used to give an algorithm for the computation of the connectivity measure. It will be

based on solving a large linear system, describing a mixed diffusion/convection process. We also introduce a novel discretization scheme to avoid the heavy directional dependency, which usually appears for discretized convection operators. PDEs in the context of diffusion MRI have been previously used for regularization [23], connectivity estimation [27], [12], [32] and fiber density estimation [25]. Our proposed PDE contains a convection operator, but in the joint position/orientation space, in [3] also convection was used for tractography, however just in position space. In [32] probabilistic tractography was put into a logical framework and an algorithm was derived which is based on solving a large linear system. This approach also works just in position space such that crossings cannot be handled adequately as long as only local neighborhoods are considered. The system matrix describes an anisotropic diffusion process.

## II. METHOD

Apart from a few examples most methods to estimate brain connectivity are based on the walker principle. Fiber tracts are initiated from certain seed points and are iteratively built by following locally defined directions. While the deterministic tracking approaches are more used for illustrative purposes, the probabilistic ones are more related to quantitative connectivity analysis. The mathematical principle behind both approaches is an integration of streamlines along the underlying data. In probabilistic tracking the process can be seen as a Markov process. The iteration process is simple: if we call  $\mathbf{s}(t)$  the current state of the tracker at step  $t$ , then the next state  $\mathbf{s}(t+1)$  is drawn from some transition probability density  $W(\mathbf{s}(t+1)|\mathbf{s}(t))$ , which may depend in some way on the DW-measurement. This process is basically a random walk in the state space of the tracker. If  $W$  is Gaussian, it is possible to formulate the limit for very small time steps, which results in a Wiener process, which we will now concentrate on.

### A. Wiener Process

In physics and mathematics there exists a huge collection of concepts for the analysis and characterization of Wiener random walkers. Basically, there are three perspectives which are mostly equivalent.

The first one, which is closest to the above described Markov process is the concept of stochastic calculus and stochastic differential equations (SDE) [31]. In physics,

SDEs are usually written as Langevin equations, which do not have the strong mathematical footing of a SDE, but are simpler to read and more similar to ordinary calculus. To give an example (actually this example already covers everything we need later) we want to consider a simple diffusion process with some additional drift. Let the state of the 'tracker' be  $\mathbf{s} \in \mathbb{R}^3$  and  $\mathbf{v}$  a vector field causing the drift. Then, the corresponding Langevin equation is

$$\dot{\mathbf{s}}(t) = \mathbf{v}(\mathbf{s}(t)) + \eta(t) \quad (1)$$

where  $\eta$  stands for mean free white noise with variance  $\sigma^2$  per unit time. It is uncorrelated in time, meaning  $\langle \eta(t)\eta(t') \rangle = \sigma^2 \delta(t-t')$ . The dot in  $\dot{\mathbf{s}}$  means time differentiation. An approximative numerical integration gives rise to the following propagation scheme:

$$\mathbf{s}(t + \Delta t) = \mathbf{s}(t) + \mathbf{v}(\mathbf{s}(t))\Delta t + \mathbf{u}(t)\sqrt{\Delta t}. \quad (2)$$

The first term  $\mathbf{v}(\mathbf{s}(t))\Delta t$  looks like ordinary Euler integration. The second, stochastic term  $\mathbf{u}(t)$  is drawn independently for each time step from  $\mathcal{N}(0, \sigma^2)$ . The factor  $\sqrt{\Delta t}$  expresses the fact that the process  $\eta(t)$  is not differentiable: variances add up and not standard deviations. Note the difference between the continuous Wiener process  $\eta(t)$  and the discrete process  $\mathbf{u}(t)$  which is just defined at discrete time points  $k\Delta t$ . Both are related by  $\int_{t-\Delta t}^t \eta(t)dt = \mathbf{u}(t)\sqrt{\Delta t}$ . The transition probability  $W$  as described in the beginning for the discrete process described in (2) is a Gaussian  $W(\cdot|\mathbf{s}(t)) = \mathcal{N}(\mathbf{s}(t) + \Delta t \mathbf{v}(\mathbf{s}(t)), \Delta t \sigma^2)$ .

The second perspective describes expectation values of an ensemble  $\mathcal{S}$  of random walkers described by (1). Suppose we have generated such an ensemble  $\mathcal{S}$  of walkers all starting at  $\mathbf{s}(0) = \mathbf{x}_0$  and we want to know the distribution of the states at some time  $T$ , i.e.

$$p_T(\mathbf{x}|\mathbf{x}_0) = \sum_{\{\mathbf{s}\} \in \mathcal{S}} \delta(\mathbf{s}(T) - \mathbf{x}) \quad (3)$$

Note, that the sum ranges over complete random walks or paths. To make this formally more transparent we always write curly brackets whenever we refer to a path (a chain of states of a walker) as a whole and not just a particular state at a specific time. In fact, the distribution described in (3) is a solution of a partial differential equation, which is called the Fokker-Planck equation (FPE) and is the master equation of the proposed continuous stochastic process. For this example, the FPE takes the form

$$\dot{p}_t = -\nabla \cdot (\mathbf{v}p_t) + \frac{\sigma^2}{2} \Delta p_t = \mathcal{H}p_t \quad (4)$$

where  $\nabla$  is the usual gradient operator in  $\mathbb{R}^3$  and  $\Delta$  the Laplacian. If we integrate this equation with respect to the initial condition  $p_0(\mathbf{x}|\mathbf{x}_0) = \delta(\mathbf{x} - \mathbf{x}_0)$  we just resemble the distribution given in (3). The function  $p_T(\mathbf{x}|\mathbf{x}_0)$  is also known as the propagator or Green's function of the corresponding stochastic process. It can formally be written as  $p_t = \exp(\mathcal{H}t)$ . Note that  $p_T(\mathbf{x}|\mathbf{x}_0)$  does not necessarily need to be normalized like a probability, e.g. walkers can die at the boundaries, which manifests in the boundary conditions of the corresponding FPE. The

proposed algorithm will be based on discretized solutions of the steady state solutions of a symmetrized FPE.

The third perspective is the path integral concept. From the viewpoint of a brain connectivity, the theory of path integrals is probably the most appealing one, however, they are probably the mathematical least understood concept and do not give a constructive way for designing an algorithm. However, it is essential for the understanding of what we are actually doing. The idea is to compute  $p_T(\mathbf{x}|\mathbf{x}_0)$  by summing over *all* path starting at  $\mathbf{x}_0$  and ending at  $\mathbf{x}$  weighted by its probability. For a rough derivation and motivation recall the discrete time representation. To compute the total probability that a particular path is drawn we take the product along the path

$$P(\mathbf{s}(N\Delta t), \dots, \mathbf{s}(\Delta t)|\mathbf{s}(0) = \mathbf{x}_0) = \prod_{i=1}^N W(\mathbf{s}(i\Delta t)|\mathbf{s}((i-1)\Delta t)),$$

but note that  $W$  is a probability *density*. So, it is not totally correct to just multiply them, the problem will be discussed below. By taking the logarithm of the above product it can be converted into a sum and in the continuous time limit  $N \rightarrow \infty$  with  $N\Delta t = T$  we have the integral form

$$-\log(P(\{\mathbf{s}\}|\mathbf{s}(0) = \mathbf{x}_0)) = -\int_0^T \log(W(\mathbf{s}(t), \dot{\mathbf{s}}(t)))dt$$

The functional  $L(\mathbf{s}(t), \dot{\mathbf{s}}(t)) = -\log(W(\mathbf{s}(t), \dot{\mathbf{s}}(t)))$  is sometimes called the Onsager-Machlup functional ([14], [7], [15], [1]) or, in the style of mechanics, the Lagrangian. It describes the cost of a path. Let us further follow the naive way and use (2) and the corresponding  $W$  to compute  $L$ . By disregarding the normalization constant (which actually diverges in the limit), we can show that

$$L_{\text{sym}}(\mathbf{s}, \dot{\mathbf{s}}) = \frac{1}{2\sigma^2} (\dot{\mathbf{s}} - \mathbf{v}(\mathbf{s}))^2 \quad (5)$$

which seems to be plausible but is wrong. The correct answer is

$$L(\mathbf{s}, \dot{\mathbf{s}}) = \frac{1}{2\sigma^2} (\dot{\mathbf{s}} - \mathbf{v}(\mathbf{s}))^2 + \frac{1}{2} (\nabla \cdot \mathbf{v})(\mathbf{s}) \quad (6)$$

The error is coming from the faulty assumption that we can simply multiply the conditional transition densities  $W$  to get the total probability, which leads to the diverging normalization constant and the missing term  $\nabla \cdot \mathbf{v}$ . Actually we have to consider some small volumes instead of infinitesimal points. We have to consider the portion of walkers starting in a volume around  $\mathbf{s}((i-1)\Delta t)$  and arriving in a volume around  $\mathbf{s}(i\Delta t)$ . This leads to an additional factor  $(1 + \frac{\Delta t \nabla \cdot \mathbf{v}}{2})$  which is the infinitesimal volume change during time  $\Delta t$  caused by the drift  $\mathbf{v}$ . In more rigorous derivations of this result the factor is justified by the Jacobian of a change of variables ([6], [18]), or by the considering the most probable tube around the path ([7]).

Let us consider the final equation stating that the probability for a walker starting at  $\mathbf{s}(0) = \mathbf{x}_0$  and arriving

at  $\mathbf{s}(T) = \mathbf{x}$  is the sum over all paths connecting this two points weighted by their probabilities

$$p_T(\mathbf{x}|\mathbf{x}_0) = \sum_{\{\mathbf{s}\} \in \mathcal{P}_T^{(\mathbf{x}|\mathbf{x}_0)}} \exp\left(-\int_0^T L(\mathbf{s}, \dot{\mathbf{s}}) dt\right) \quad (7)$$

where  $\mathcal{P}_T^{(\mathbf{x}|\mathbf{x}_0)}$  denotes the set of all paths of length  $T$  starting in  $\mathbf{x}_0$  and terminating at  $\mathbf{x}$ . In fact, the *sum* over all path is an integration in a functional space, for more details see e.g. [8], [18], [31]. For convenience we omit to write here any normalization constant and assume that the measure is appropriately normalized.

### B. Reversibility and Symmetry

In fact, the additional term  $(\nabla \cdot \mathbf{v})/2$  in (6) is quite important for us, because it is responsible for the fact that the described random walk is irreversible ([11]). In the context of brain connectivity this is directly related to the symmetry of the connectivity measure, so we will detail this out now. If we call  $L'$  the Lagrangian with negative velocities  $\mathbf{v} \mapsto -\mathbf{v}$  and  $\mathbf{s}'(t) = \mathbf{s}(T-t)$  the path traversed in opposite direction. Then, it is easy to see that  $\int L'(\mathbf{s}', \dot{\mathbf{s}}') dt \neq \int L(\mathbf{s}, \dot{\mathbf{s}}) dt$  with the  $L$  obtained in (6). This also leads to  $p_T(\mathbf{x}|\mathbf{x}_0) \neq p'_T(\mathbf{x}_0|\mathbf{x})$ . This asymmetry is basically caused by drift together with particle conservation. Considering the corresponding FPE in (4) makes it more clear. While the diffusion term  $\Delta$  is symmetric (selfadjoint, see Appendix IV-A for definition), the convection/drift is not antisymmetric, i.e. the operator  $\mathcal{H}'$  corresponding to the flipped Lagrangian  $L'$  is not equal to adjoint operator  $\mathcal{H}^+$  which has to be case to fulfill  $p_T(\mathbf{x}|\mathbf{x}_0) = p'_T(\mathbf{x}_0|\mathbf{x})$ . However, for  $L_{\text{sym}}$  everything is different. In fact, we have

$$\int_0^T L'_{\text{sym}}(\mathbf{s}', \dot{\mathbf{s}}') dt = \int_0^T L_{\text{sym}}(\mathbf{s}, \dot{\mathbf{s}}) dt$$

which should also lead to a symmetric propagator  $p_T(\mathbf{x}|\mathbf{x}_0) = p'_T(\mathbf{x}_0|\mathbf{x})$ . But how to compute (7) for  $L_{\text{sym}}$  in practice, what is the corresponding FPE? The term  $\nabla \cdot \mathbf{v}$  acts like an additional potential energy. In fact, the Feynman-Kac (FK) formula [17] tells us that such a potential can be directly integrated into the FPE: suppose we have a given Lagrangian  $L$  together with its path integral and a corresponding FPE with operator  $\mathcal{H}$ . For a potential field  $V(\mathbf{s})$  we define a new  $L'(\mathbf{s}, \dot{\mathbf{s}}) = L(\mathbf{s}, \dot{\mathbf{s}}) - V(\mathbf{s})$ , then the FK formula tells us that the corresponding FPE operator is just  $\mathcal{H}' = \mathcal{H} + V$ . Applying this our problem with  $V = (\nabla \cdot \mathbf{v})/2$  gives

$$\begin{aligned} \mathcal{H}_{\text{sym}} p &= \mathcal{H} p + \frac{1}{2} (\nabla \cdot \mathbf{v}) p \\ &= \frac{\sigma^2}{2} \Delta p + \frac{1}{2} (\nabla \cdot \mathbf{v}) p - \nabla \cdot (\mathbf{v} p) \\ &= \frac{\sigma^2}{2} \Delta p - \frac{1}{2} (\mathbf{v} \cdot \nabla p + \nabla \cdot (\mathbf{v} p)) \end{aligned}$$

From the last line we can also see the symmetry property of  $\mathcal{H}_{\text{sym}}$ . The convection part  $\nabla \cdot (\mathbf{v} p) + \mathbf{v} \cdot \nabla p$  is antisymmetric in the sense of the operator adjoint and hence the operator  $\mathcal{H}'_{\text{sym}}$ , which corresponds to flipped

velocities, is just the adjoint of  $\mathcal{H}_{\text{sym}}$ . One can also see that the particle conservation is lost: we cannot write  $\mathcal{H}_{\text{sym}}$  as the a divergence of something. Note the similarity of  $\mathcal{H}_{\text{sym}}$  with the quantum mechanical Hamiltonian of a particle in a vector potential, which is up to some constants  $(i\nabla - \mathbf{v})^2 = -\Delta - i(\nabla \mathbf{v} - \mathbf{v} \nabla) + \mathbf{v}^2$ . In quantum mechanics the Hamiltonian is indeed self-adjoint due to the additional complex unit in front of the anti-symmetric part.

### C. Steady States and Path Trails

Up to now we have considered only paths with some specific length  $T$ . However, we are interested in *all* path without any length restriction. That is, we sum up over all paths connecting  $\mathbf{x}_0$  and  $\mathbf{x}$  of arbitrary length to get a density  $p(\mathbf{x}|\mathbf{x}_0)$  which is independent of  $T$ , i.e.

$$\begin{aligned} p(\mathbf{x}|\mathbf{x}_0) &= \int_0^\infty dT p_T(\mathbf{x}|\mathbf{x}_0) \\ &= \sum_{\{\mathbf{s}\} \in \mathcal{P}^{(\mathbf{x}|\mathbf{x}_0)}} e^{-\int_0^T L(\mathbf{s}, \dot{\mathbf{s}}) dt} \end{aligned}$$

where  $\mathcal{P}^{(\mathbf{x}|\mathbf{x}_0)}$  is the set of paths of any length connecting  $\mathbf{x}_0$  with  $\mathbf{x}$ . With the assumption  $\lim_{T \rightarrow \infty} p_T(\mathbf{x}|\mathbf{x}_0) = 0$ , i.e. all walkers eventually die, the function  $p(\mathbf{x}|\mathbf{x}_0)$  is the steady state solution of the corresponding FPE, i.e.  $p(\mathbf{x}|\mathbf{x}_0)$  is the solution of the equation

$$-\mathcal{H} p(\mathbf{x}|\mathbf{x}_0) = \delta(\mathbf{x} - \mathbf{x}_0).$$

This is the basic type of equation we will solve to estimate brain connectivities. In the following we call  $p(\mathbf{x}|\mathbf{x}_0)$  the connectivity amplitude. From ordinary probabilistic tractography we know the so called length bias. With increasing euclidean distance, connectivity values decrease dramatically, usually exponentially. To account for this bias a linear reweighing was proposed in [4], that is,

$$p_{\text{lin}}(\mathbf{x}|\mathbf{x}_0) = \int_0^\infty dT T p_T(\mathbf{x}|\mathbf{x}_0). \quad (8)$$

We will see later how  $p_{\text{lin}}$  can be computed in practice. Due to the exponential decrease one could also tend to use exponential corrections, i.e. use

$$p_\kappa(\mathbf{x}|\mathbf{x}_0) = \int_0^\infty dT e^{\kappa T} p_T(\mathbf{x}|\mathbf{x}_0) \quad (9)$$

with positive  $\kappa \in \mathbb{R}$ . In fact, this results in a spectral shift of the operator  $\mathcal{H} \mapsto \mathcal{H} + \kappa$ . Of course, the choice of  $\kappa$  is difficult. Large  $\kappa$  will cause bad condition numbers for  $\mathcal{H}$  and, in the extreme case, lead to a diverging  $p_\kappa(\mathbf{x}|\mathbf{x}_0)$ .

Until now, we were interested in a measure how strong two points  $\mathbf{x}_1$  and  $\mathbf{x}_0$  are connected, but one might also be interested in *how* the actual connection looks like. Instead of just summing over all paths connecting two points, one can additionally image the path itself by counting how often the path visited a specific position  $\mathbf{x}$ . We call this image the trail image of a path  $\mathbf{s}$ , and it is defined by

$$\tau_{\mathbf{s}}(\mathbf{x}) = \int_0^T \delta(\mathbf{x} - \mathbf{s}(t)) dt$$

Now, we can write the mean trail image of a path connecting two point  $\mathbf{x}_1$  and  $\mathbf{x}_2$  by the expectation value

$$\bar{\tau}_{(\mathbf{x}_1|\mathbf{x}_0)}(\mathbf{x}) = \sum_{\{\mathbf{s}\} \in \mathcal{P}(\mathbf{x}|\mathbf{x}_0)} \tau_{\mathbf{s}}(\mathbf{x}) e^{-\int_0^T L(\mathbf{s}, \dot{\mathbf{s}}) dt}.$$

In order to compute  $\bar{\tau}$  we have to use the so called Einstein-Smoluchowski-Kolmogorov-Chapman (ESKC) relation, or simply semigroup property, which tells that the path-integral, or the corresponding propagator can always be split like

$$p_T(\mathbf{x}_1|\mathbf{x}_0) = \int d\mathbf{x}' p_{T-t'}(\mathbf{x}_1|\mathbf{x}') p_{t'}(\mathbf{x}'|\mathbf{x}_0)$$

for any given intermediate point  $0 < t' < T$ . This means we can slice the propagator at any given length  $t'$  and consider all possible intermediate positions  $\mathbf{s}(t') = \mathbf{x}'$  the path has at  $t'$  and integrate over them by accounting for the probability of the path to get from  $\mathbf{x}_0$  to  $\mathbf{x}'$  and to reach the target  $\mathbf{x}_1$  starting from  $\mathbf{x}'$ . To compute  $\bar{\tau}$  we first consider the point density of the path at some specific length  $t'$ . That is, we count how often a path traverses the point  $\mathbf{x}$  at length  $t'$  by

$$\begin{aligned} \rho_{T,t'}(\mathbf{x}) &= \int d\mathbf{x}' \delta(\mathbf{x} - \mathbf{x}') p_{T-t'}(\mathbf{x}_1|\mathbf{x}') p_{t'}(\mathbf{x}'|\mathbf{x}_0) \\ &= p_{T-t'}(\mathbf{x}_1|\mathbf{x}) p_{t'}(\mathbf{x}|\mathbf{x}_0) \end{aligned}$$

If we integrate now  $\rho_{t',T}$  over all intermediate times  $0 < t' < T$  and, again, integrate this over all possible  $0 < T < \infty$  we get the mean trail image

$$\bar{\tau}_{(\mathbf{x}_1|\mathbf{x}_2)}(\mathbf{x}) = \int_0^\infty dT \int_0^T dt' \rho_{T,t'}(\mathbf{x})$$

Plugging this altogether gives the simple final result

$$\bar{\tau}_{(\mathbf{x}_1|\mathbf{x}_0)}(\mathbf{x}) = p(\mathbf{x}_1|\mathbf{x}) p(\mathbf{x}|\mathbf{x}_0)$$

and, as we already know how to compute  $p$  we are ready. Further note that

$$\begin{aligned} \int d\mathbf{x} \bar{\tau}_{(\mathbf{x}_1|\mathbf{x}_0)}(\mathbf{x}) &= \int_0^\infty dT T p(\mathbf{x}_1|\mathbf{x}_0) \\ &= p_{\text{lin}}(\mathbf{x}_1|\mathbf{x}_0), \end{aligned}$$

that is, if we integrate the mean trail image, we just get the linearly reweighed version of (8) and have also a way to compute (8) in practice.

#### D. Application to DW-MRI data

All concepts were introduced by considering a 3D diffusion process with drift. But, how to apply this kind of stochastic process for brain connectivity analysis? The data is basically tensor-like, meaning it is point symmetric, there is no velocity field available. Even when we have orientation distributions, there is still no convection-like force. So, what to do?

First of all, we have to realize that usual probabilistic tracking algorithms are not Markovian with respect to the position  $\mathbf{r} \in \mathbb{R}^3$ . The propagation direction usually depends not just on the position, but also on the previous step made. So, the state space of the tracker should be the

joint space of position and orientation  $\mathbf{s} = (\mathbf{r}, \mathbf{n})$ , where  $\mathbf{r} \in \mathbb{R}^3$  and  $\mathbf{n} \in S_2$ . The data we get from the diffusion measurement is basically an fiber orientation distribution  $f(\mathbf{r}, \mathbf{n})$  defined on this joint position/orientation space. In fact, in this joint space there are several ways to define meaningful connectivity measures. We propose to use the following Lagrangian

$$L(\mathbf{r}, \dot{\mathbf{r}}, \mathbf{n}, \dot{\mathbf{n}}) = \frac{1}{2\sigma_r^2} (\dot{\mathbf{r}} - \mathbf{n}f(\mathbf{r}, \mathbf{n}))^2 + \frac{1}{2\sigma_n^2} \dot{\mathbf{n}}^2 \quad (10)$$

as path-costs. Paths with  $\dot{\mathbf{s}} \sim \mathbf{n}f$  and small changes in  $\mathbf{n}$  are assigned with small costs, and hence, with high probability. From the walker perspective, there is a convective force which drives a walker with internal state  $\mathbf{n}$  into direction  $\mathbf{n}$ , while the speed is proportional to the data term  $f$ . Additionally there is diffusion on the orientation variable, enabling the walker to change its directions, or conversely, penalizes too strong bending. Imagine the system as a network of pipes oriented in all possible directions carrying a fluid which flows with speed  $f(\mathbf{r}, \mathbf{n})$ . The flow is not perfectly convective, neighboring parallel pipes can exchange fluid (this is spatial diffusion) and also crossing pipes exchange some fluid (this is the angular diffusion). In fact, we can also let spatial diffusion  $\sigma_r \rightarrow 0$  such that there is only pure convection. However, as we will see later, the discretization of the FPE will force us to have finite values for  $\sigma_r$ .

The FPE operator is not totally straight-forward, because there is an additional term coming from the curvature of the sphere ([15], [1]). It looks like

$$\mathcal{H} = \frac{1}{2}(\sigma_r^2 \Delta_{\mathbf{r}} + \sigma_n^2 \Delta_{\mathbf{n}}) - \frac{1}{2}(\mathbf{v} \cdot \nabla_{\mathbf{r}} + \nabla_{\mathbf{r}} \cdot \mathbf{v}) + \frac{\sigma_n^2 R}{12}$$

where the velocity is defined by  $\mathbf{v}(\mathbf{r}, \mathbf{n}) = \mathbf{n}f(\mathbf{r}, \mathbf{n})$ . The additional constant  $\frac{R}{12}$  is coming from the curvedness of the sphere which is  $R = 2/\rho^2$  for a 2-sphere of radius  $\rho$ . However, there is actually no metric connection between the position space  $\mathbb{R}^3$  of the orientation space  $S_2$ . The 'radius' of the sphere  $S_2$  has no actual meaning. So, the value of  $R/12$  is rather arbitrary. In fact,  $R/12$  acts like an additional exponential weighting, like the  $\kappa$  we already introduced above and could be absorbed by that. So, we exclude  $R/12$  in the following, or, imagine  $\rho$  to be pretty large.

Let us now look at the symmetry properties of  $\mathcal{H}$ . Let  $\mathcal{Z}$  the operator that does a point reflection on some function  $a(\mathbf{r}, \mathbf{n})$  in the sense

$$(\mathcal{Z}a)(\mathbf{r}, \mathbf{n}) := a(\mathbf{r}, -\mathbf{n})$$

Then, we can easily show that

$$\mathcal{H}\mathcal{Z} = \mathcal{Z}\mathcal{H}^+$$

because the data  $f$  is symmetric  $\mathcal{Z}f = f$ . In other words, the operator  $\mathcal{H}\mathcal{Z}$  is selfadjoint. Formally we can write the connectivity amplitudes as

$$p(\mathbf{r}, \mathbf{n}|\mathbf{r}_0, \mathbf{n}_0) = -\langle e_{(\mathbf{r}, \mathbf{n})} | \mathcal{H}^{-1} e_{(\mathbf{r}_0, \mathbf{n}_0)} \rangle$$

where  $e_{(\mathbf{r}', \mathbf{n}')}(\mathbf{r}, \mathbf{n}) = \delta(\mathbf{r}' - \mathbf{r})\delta(\mathbf{n}' - \mathbf{n})$ . For the connectivity amplitude the symmetry means

$$p(\mathbf{r}, \mathbf{n}|\mathbf{r}_0, \mathbf{n}_0) = p(\mathbf{r}_0, -\mathbf{n}_0|\mathbf{r}, -\mathbf{n}),$$

because  $\mathcal{H}^{-1} = \mathcal{Z}(\mathcal{H}^+)^{-1}\mathcal{Z}$ .

If we now think of some function  $a(\mathbf{r}, \mathbf{n})$  describing a seed point density, and  $b(\mathbf{r}, \mathbf{n})$  a terminal point density. For both we can think of indicator functions describing some cortical region of interests. Then, we can define the symmetric connectivity measure  $c(a, b)$  to be

$$c(a, b) = -\langle a|\mathcal{Z}\mathcal{H}^{-1}|b\rangle$$

which can be written in terms of the connectivity amplitudes  $p(\mathbf{r}, \mathbf{n}|\mathbf{r}_0, \mathbf{n}_0)$  as

$$c(a, b) = \int \int a(\mathbf{r}, -\mathbf{n})p(\mathbf{r}, \mathbf{n}|\mathbf{r}_0, \mathbf{n}_0)b(\mathbf{r}_0, \mathbf{n}_0)$$

So,  $c(a, b)$  is the path integral over all path connecting region  $a$  with region  $b$  according to the Lagrangian  $L$ . Accordingly, we can also define  $c^\kappa$  and  $c^{\text{lin}}$  corresponding to  $p_{\text{lin}}$  in equation (8) and  $p_\kappa$  in equation (9), respectively. The path trail image is

$$\begin{aligned} \bar{\tau}_{(a|b)}(\mathbf{r}, \mathbf{n}) &= \langle a|\mathcal{H}^{-1}e_{\mathbf{r}, \mathbf{n}}\rangle\langle e_{\mathbf{r}, \mathbf{n}}|\mathcal{H}^{-1}b\rangle \\ &= \langle e_{\mathbf{r}, \mathbf{n}}|\mathcal{Z}\mathcal{H}^{-1}\mathcal{Z}a\rangle\langle e_{\mathbf{r}, \mathbf{n}}|\mathcal{H}^{-1}b\rangle \\ &= \langle e_{\mathbf{r}, -\mathbf{n}}|\mathcal{H}^{-1}\mathcal{Z}a\rangle\langle e_{\mathbf{r}, \mathbf{n}}|\mathcal{H}^{-1}b\rangle \end{aligned}$$

Note that  $\mathcal{Z}\bar{\tau}_{(a|b)} = \bar{\tau}_{(\mathcal{Z}b|\mathcal{Z}a)}$ .

Usually the seed functions  $a$  and  $b$  do not depend on  $\mathbf{n}$  because we do not have any preference for the starting orientation, so  $\mathcal{Z}a = a$  and  $\mathcal{Z}b = b$ . Several relationships are then simplified, e.g.  $\mathcal{Z}\bar{\tau}_{(a|b)} = \bar{\tau}_{(b|a)}$  and  $c(a, b) = \langle a|\mathcal{H}^{-1}|b\rangle$ . For the special case if  $a_{\mathbf{r}_0}(\mathbf{r}, \mathbf{n}) = \delta(\mathbf{r} - \mathbf{r}_0)$  we can also define the connectivity measure between two spatial locations  $\mathbf{r}$  and  $\mathbf{r}_0$  as

$$c(\mathbf{r}_0, \mathbf{r}_1) = c(a_{\mathbf{r}_0}, a_{\mathbf{r}_1}) \quad (11)$$

In all experiments we will report the normalized connectivity amplitudes

$$c_n(a, b) = \frac{c(a, b)}{\sqrt{c(a, a)c(b, b)}}$$

which is quite natural and reminds one of Pearson's correlation coefficient.

### E. Angular Constraints, the Data Term and Boundary Conditions

The Lagrangian (10) penalizes bending, which is a good prior for straight fibers, but underestimates curved fibers. In [4] this problem does not appear, because the walker is always back projected onto the nearest fiber direction in a voxel. Such a behavior cannot be realized by a Wiener process. However, we can mimic such a behavior by an angular constraint such that the walkers do not deviate too strong from the main fiber directions. That is, we only simulate paths where  $\mathbf{n}$  is not too far away from the main fiber directions, which is similar to the maximum angle thresholds known from ordinary streamline algorithms,

but not so rigorous (it is still possible to find paths where the spatial tangent  $\dot{\mathbf{r}}$  to the path is not perfectly  $\mathbf{n}$ ). Now, we are able to set  $\sigma_n$  pretty large, i.e. low penalty on bending, but the walker will be along the main fiber directions. In fact, this idea will also help to keep the running time and memory consumption of our algorithm in a reasonable range, because we only have to simulate the domain in the neighborhood of the fiber directions and not on the complete sphere. Note that the angular constraint may also be seen as an additional cost in the Lagrangian, i.e. the forbidden path are assigned with infinite costs.

There are lots of ways to determine the speed function  $f$ , which represents the DW-data. For example, we could directly use the fiber orientation distributions (FOD), e.g. estimated by spherical deconvolution [28]. Or, one could estimate the main fiber directions by a local maxima detection of an FOD, and use them as anchor directions to construct the speed function. We opt for latter, primarily because the angular constraints can be much better controlled. Let  $\mathbf{d}_i$  be the local maximas of the FOD. Then, we construct the speed function by

$$f(\mathbf{n}) = \sum_{i=1}^N (\mathbf{n} \cdot \mathbf{d}_i)^{2n} \quad (12)$$

with some fixed  $n > 0$ . The simulation domain is now defined by thresholding this speed function, i.e. we only consider regions with  $f > \epsilon$  for some  $\epsilon > 0$ .

To solve the FPE we have to set some boundary conditions. It is natural to let the walkers die once they touch the boundary of the domain, which is equivalent to a zero Dirichlet conditions at the boundary. So the complete problem we want to solve is

$$-\mathcal{H}p = a \quad \text{where} \quad p(\partial\Omega) = 0 \quad (13)$$

where  $\partial\Omega$  denotes the boundary of the simulation domain,  $p$  the unknown steady state solution and  $a$  the seed region where the walkers are emitted. Of course, other boundary condition, like Neumann conditions, might be applied, for example at the transitions to the ventricles. However, we restrict here all considerations to the simple Dirichlet conditions.

### F. Implementation, Discretization and Solver

In order to solve the equation  $-\mathcal{H}a = b$  we have to discretize the operator  $\mathcal{H}$ . The convective part of  $\mathcal{H}$  makes this a pretty hard problem, usual Finite Element Methods are only applicable for diffusion dominated problems. So, we decided to use a finite difference upwind-downwind scheme. However, such schemes are known to introduce errors (known as false diffusion) when the convection direction is not aligned with the underlying discretization grid. In particular for steady state solutions these problems become severe and the solutions show heavy orientation dependency. Fortunately our problem is special, the convection direction is always fixed for a volume  $p(\mathbf{r}, \mathbf{n})$  with fixed  $\mathbf{n}$ , namely  $\mathbf{n}$ . So, we propose to steer the grid for each direction along the current convection direction.

Practically, we discretize the sphere into  $N$  direction homogeneously distributed over the full sphere (in the experiments we used  $N = 128$  directions). So, we have  $N$  volumes, where the discretization grid of the volume associated with the  $i$ th direction  $\mathbf{n}_i$  is steered such that one of the coordinate axis is along direction  $\mathbf{n}_i$ . In this way we are able to produce quite clean convection, however the angular diffusion gets disturbed. A voxel at some discrete coordinate in volume  $i$  does not have a unique partner in volume  $j$  at exactly the same discrete position. We need this partner in order to implement the spherical Laplace-Beltrami operator  $\Delta_{\mathbf{n}}$ , which only acts on the spherical coordinate. The simplest way to account for that is to use trilinear interpolation, which, unfortunately causes another unwanted spatial diffusion effect. However, this false diffusion is not so disturbing: it is independent of the orientation and the error is proportional to the angular diffusion and not to the speed function. Second, we can reduce the error by a finer discretization of the spatial grid. We quantified this additional spatial diffusion in an experiment and found that a angular displacement of  $\pi = 180^\circ$  (for a  $N = 128$  points on the sphere) causes an additional spatial displacement of about 5 spatial grid units, i.e. the cost of a  $180^\circ$  turn on the spot compares to a 5 voxel jump. So, for some given theoretical  $\sigma_n$  and  $\sigma_r$ , the actual  $\sigma_r^{\text{act}}$  turns out to be approximately  $\sigma_r^{\text{act}} = \sqrt{\sigma_r^2 + (\sigma_n 5/\pi)^2}$ , if  $\sigma_r$  is given in grid units. As this is already pretty much we decided to set the theoretical  $\sigma_r$  to zero in all experiments. In general, for arbitrary number of points on the sphere, we found the approximation  $\sigma_r^{\text{act}} = \sqrt{\sigma_r^2 + (\sigma_n \sqrt{N}/7)^2}$ , i.e. with a finer sphere discretization the effects get stronger. But again, note that the 'physical' amount of this false diffusion depends also on the spatial grid size. All the gritty details about the discretization scheme are given in Appendix IV-B.

The whole matrix is scattered with MATLAB's sparse matrix capabilities. To solve the discretized equation (13) we found the GMRES algorithm the most stable and efficient [26], we just used the MATLAB's `gmres` command. As number of restarts we used 5. The tolerance value is set to  $10^{-6}$  in all experiments. The running time depends on the size of the problem. If we use the setting as described below in the experiments we get usually a system with about  $2-3 \cdot 10^6$  variables, which is scattered in 1-2 minutes on a common Desktop PC (Intel I7, 16GB). Solving the equation also takes about one minute.

### III. EXPERIMENTS

We want to begin with a small demonstration of the proposed discretization scheme. Let  $\mathbf{d}$  some arbitrary direction and the speed function is constructed according to (12) with  $n = 25$  and  $\epsilon = 0.02$ . In Figure 1 we choose  $\mathbf{d} = (\cos(\varphi), \sin(\varphi), 0)$  with  $\varphi = 0.3\pi$  (a,b,e) and  $\varphi = \pi$  (c,d,f). Further we choose  $\sigma_r = 0$  and  $\sigma_n = \pi/12$ . Figure 1 (a-d) shows the solution to (13) with  $a(\mathbf{r}, \mathbf{n}) = \delta(\mathbf{r} - \mathbf{r}_0)$  where  $\mathbf{r}_0$  is located in the lower left corner of the simulation domain. The spatial intensity maps in Figure 1 show the solution

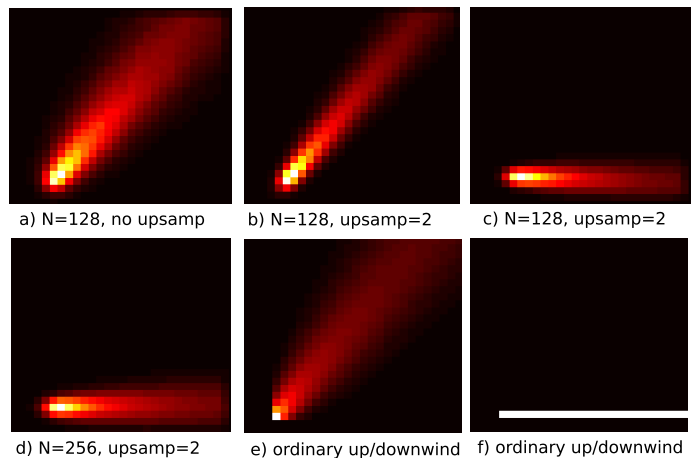


Fig. 1. Demonstration of the proposed discretization scheme. In (a-d) the novel scheme for different granularities are shown. In (e-f) the ordinary scheme is shown for comparison.

$p$  integrated over the angular variable  $\int_{S_2} p(\mathbf{r}, \mathbf{n}) d\mathbf{n}$ , i.e. we actually show the connectivity amplitudes  $c(\mathbf{r}, \mathbf{r}_0)$  as defined in (11). The matrix size is of size  $30 \times 30 \times 7$ . In Figure 1a,b,c) we used a sphere with  $N=128$  directions in (d) with  $N=256$  directions. Further, we demonstrate the effect of spatial oversampling, i.e. a upsampling by a factor of 2 means that the actual matrix size is in the range of  $60 \times 60 \times 14$  (for details see Appendix IV-B). By comparing (a) and (b) we can obviously see how the the upsampling reduces false diffusion. Similarly comparing (b), (c) and (d), we see that the amount of false diffusion does not depend on the direction, but the directions are not perfect due to the discretization of the sphere. For comparison we also simulated an ordinary up/downwind scheme in (e),(f) with  $\sigma_n = \sigma_r = 0$ . The amount of false diffusion depends dramatically on the direction.

#### A. Numerical Phantom

For further demonstration we constructed a numerical phantom consisting of crossing and bending configurations (see Figure 2d)). Six seed locations  $\mathbf{r}_1, \dots, \mathbf{r}_6$  were selected such that they are pairwise connected as (1-2), (3-4) and (5-6). We did not simulate the MR-signal, but created the underlying directions directly. The directions  $\mathbf{d}_i$  are created continuously (not aligned with the discretized sphere directions), and a pseudo FOD is generated using  $\sum_i \exp(\alpha((\mathbf{d}_i \mathbf{n})^2 - 1))$ , which is shown in Figure 2d). For robustness analysis we distorted the directions by Gaussian noise of standard deviation  $\sigma_{\text{nz}}$ .

Figure 2a-c) gives some first results of our approach. We show the connectivity amplitudes  $c(\mathbf{r}, \mathbf{r}_i)$  as images, where  $\mathbf{r}_i$  is one of the fixed seed point. Figure 2a) shows  $c$  without noise and b) with noise ( $\sigma_{\text{nz}} = 0.1$ ). Figure 2c) shows the same experiment but with exponential length bias correction of  $\kappa = 0.01$ . Examples for the path trails images are shown in Figure 2e) that correspond to the experiment in Figure 2b). Trail images for all pairs of

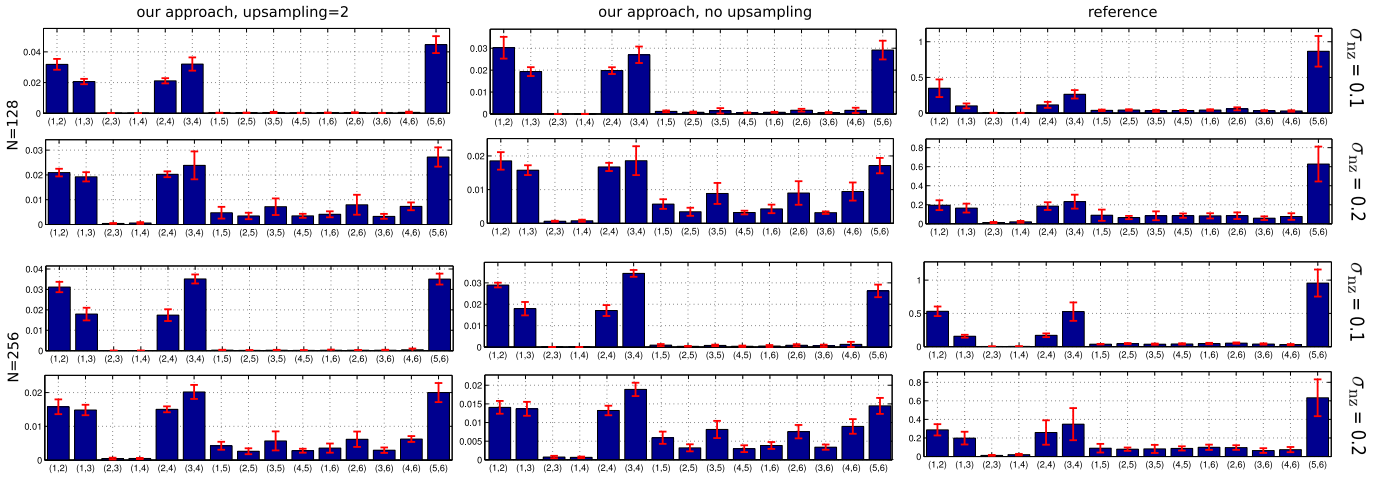


Fig. 3. Quantitative analysis of connectivity values (c-values) over 50 trials. The barplots show mean c-values together with standard deviation. The x-axis indicate all possible seed pairs  $(i, j)$  for  $i, j = 1, \dots, 6$  of the numerical phantom.

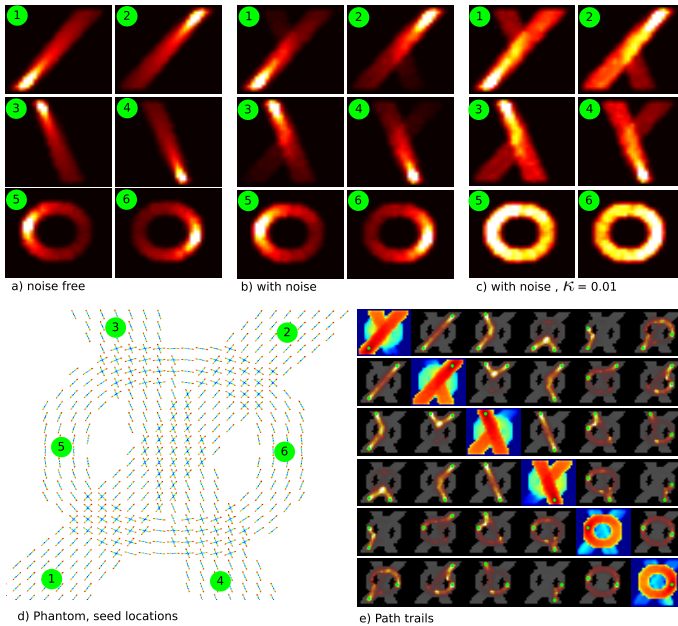


Fig. 2. In (a-c) connectivity amplitudes for three different settings are shown, the color scaling is fixed and the same for all three settings. In (d) the FOD of the phantom together with the seed locations is given, and (e) shows the matrix of all possible path trails together with the connectivity amplitudes in logarithmic scaling in the diagonal.

seed combinations are shown, the diagonal shows again the connectivity amplitudes but in logarithmic scaling.

To get a quantitative picture we repeated the above experiment for different noise levels  $\sigma_{nz} = 0.1, 0.2$  and different discretization scheme, namely spherical discretization with  $N = 128$  and  $N = 256$  directions and with and w/o spatial upsampling (with a factor of 2). Additionally, the orientation of the discrete sphere was randomly changed for each run. As reference approach we followed [4] (for details see Appendix IV-C), with  $\Delta s = 1, \sigma = 0.2$ , without revisits and with length bias correction. Figure 3

shows barplots of the normalized connectivity amplitudes  $c_n(\mathbf{r}_i, \mathbf{r}_j)$  for all pairs of seeds averaged over 50 runs together with the standard deviation.

### B. In-Vivo Human Brain

To investigate our approach on real DTI data we considered 28 scans of healthy volunteers at a b-value of  $1\text{ms}/\mu\text{m}^2$  with 61 diffusion directions and an isotropic resolution of  $2\text{mm}^3$ . A white matter probability map was generated with SPM (Version 8, <http://www.fil.ion.ucl.ac.uk/spm/>, [10]) on a T1-weighted scan, which was co-registered to the  $b_0$ -scan of the diffusion sequence. For each subject the scans were repeated two times (in two different sessions) to allow to investigate the robustness of the approach. To compute the FOD a constrained spherical deconvolution was used together with a  $L_1$ -regularizer [20]. The fiber response function (FRF) was chosen as  $FRF(\mathbf{n}) = \exp(-bD_1(n_i^{\text{fib}}n_i)^2)$  with  $D_1 = 1\mu\text{m}^2/\text{ms}$  for all subjects and reconstructed on a  $N = 128$  sphere. The local maximas of the FOD are determined by fitting a quadratic form to the neighborhood of the discrete local maxima (the same approach as used in [23]). Spurious local maximas were filtered out by neglecting all maximas smaller than 20% of the global one. The speed function is constructed in the same way as for the numerical phantom. The spherical discretization is kept at  $N = 128$  and no spatial up sampling is applied. The probabilistic white matter segmentation of SPM was thresholded at 0.5 and used as white matter mask. To compare and analyze the group, the AAL atlas [30] was registered to the subjects' native space, normalization was done with SPM 8. The first 90 ROIs (distributed over the neocortex) of the AAL atlas were used to compute connectivity matrices.

Figure 4a-e) show examples of the mean connectivity matrices (CM) over the whole group. The first 45 ROIs belong to the right hemisphere, the last 45 the right hemisphere. The CM is shown in logarithmic scaling. To

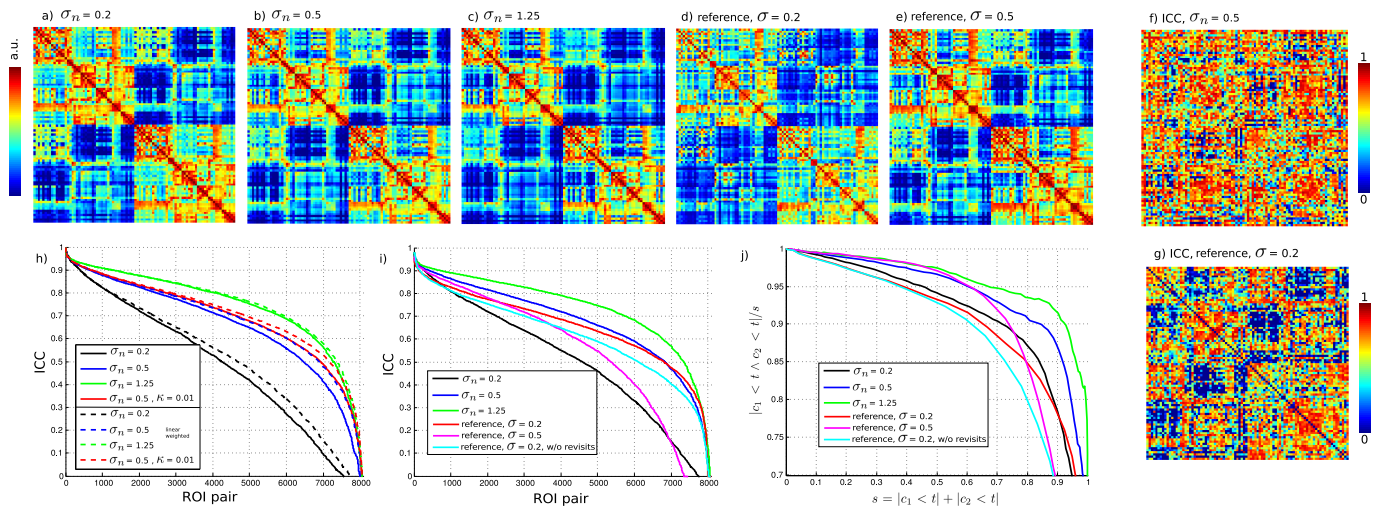


Fig. 4. In (a-e) average connectivity matrices (CM) for different approaches are shown. The matrices in (f,g) show ICC values for individual  $c$ -values. Plot (h,i) display the ICC for all  $c$ -values (all ROI pairs) in the CM. Plot (j) shows agreement values.

get a comparable contrast we used the following formula  $c_{\log}(a, b) = \log(t + c_n(a, b))$  where  $t$  is the 20% quantile of  $c_n$  over all regions. The CMs obtained by our approach are compared to the reference approach [4] (Figure 4d-e)). To investigate the robustness we computed the intraclass correlation coefficient (ICC)<sup>1</sup> for each connectivity value ( $c$ -value) in the CM. In Figure 4h) we show the ICC over all  $c$ -values in the CM sorted by ICC magnitude for different settings: we varied  $\sigma_n$  and show one result with exponential weighting ( $\kappa = 0.01$ ). For all results we also show the corresponding linear weighted result  $c_n^{\text{lin}}$ . Figure 4i) compares our approach with [4] with different parameters:  $\sigma = 0.2, 0.5, \Delta s = 1$ , with (w/o) revisits and length bias correction (lbc). In Figure 4f,g) we show for our approach and the reference the ICCs for the individual  $c$ -values as a matrix. Table I shows mean and median ICCs for our approach and the reference with more different settings. It is common to put thresholds to get a binary decision of connectivity. To investigate the robustness of such a thresholding operation an agreement measure is calculated as follows: let  $t$  be some threshold, then  $a = |c_1 < t \wedge c_2 < t|$  denotes the number of regions that are not connected in scan 1 and in scan 2, where the number is counted over all possible ROI pairs and subjects. The agreement value  $a$  is normalized by the total number of non-connected regions  $s = |c_1 < t| + |c_2 < t|$ , and hence,  $a/s$  is a number between 0 and 1. If we now vary over all thresholds  $t$  and plot  $a/s$  as a function of  $s$  we get plots displayed in Figure 4j).

Finally, Figure 5 shows examples of path trail images for two ROI pairs of the AAL atlas. The two ROIs are highlighted in green and blue, respectively. The white matter mask is depicted in dark gray. The path trail  $\bar{\tau}_{(a|b)}(\mathbf{r}, \mathbf{n})$

<sup>1</sup>If  $c_1$  and  $c_2$  are  $c$ -values in the CM for scan 1 and scan 2, respectively, then the ICC is  $ICC(c) = \langle (c_1 - \bar{c})(c_2 - \bar{c}) \rangle / \langle (c - \bar{c})^2 \rangle$ , where  $\langle \rangle$  denotes the expectation over the whole group and  $\bar{c} = \langle (c_1 + c_2) / 2 \rangle$ . The ICC is 1 if all the variance of the  $c$ -value can be explained by differences amongst the subjects.

TABLE I  
QUANTITATIVE COMPARISON BY ICC

Method	Mean	Median
<b>Our Approach</b>		
$\sigma_n = 0.2$	0.47	0.51
$\sigma_n = 0.5$	0.64	0.69
$\sigma_n = 1.25$	0.73	0.78
$\sigma_n = 0.5, \kappa = 0.01$	0.67	0.72
$\sigma_n = 0.2$ , lin. weighted	0.50	0.54
$\sigma_n = 0.5$ , lin. weighted	0.67	0.71
$\sigma_n = 1.25$ , lin. weighted	0.73	0.78
$\sigma_n = 0.5, \kappa = 0.01$ , lin. weighted	0.69	0.73
<b>Reference [4]</b>		
$\sigma = 0.2, \Delta s = 1$	0.65	0.68
$\sigma = 0.5, \Delta s = 1$	0.55	0.63
$\sigma = 0.2, \Delta s = 1$ , w/o revisits	0.61	0.64
$\sigma = 0.2, \Delta s = 1$ , no lbc	0.64	0.67
$\sigma = 0.2, \Delta s = 0.25$	0.55	0.58
$\sigma = 0.2, \Delta s = 0.5$	0.60	0.63

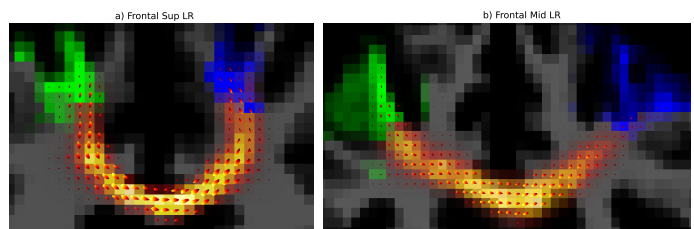


Fig. 5. Examples of mean path trails for two ROI pairs in the frontal regions. Green and Blue depict the ROIs. The path trails are shown as glyphs and averaged over directions.

is obviously a function in the joint position/orientation space, which is shown in glyph representation, but note that the glyphs are not pointsymmetric as one used to observe. The traversal direction is in this example from the blue to the green ROI.

#### IV. DISCUSSION

We proposed to use a Wiener process for the estimation of structural brain connectivities. The path integral



perspective gave us the insight why the usual random walker principle leads to asymmetric connectivities. To symmetrize the solution an additional potential was introduced, which symmetrized the path integral and the corresponding Fokker Planck equation. However, particle conservation and, hence, the usual walker perspective is lost. To solve the FPE we introduced a novel discretization scheme which avoids the directional dependency of the false diffusion introduced by the discretization of the convection operator.

Initial experiments (in Figure 1) show that the new discretization approach is valid. In Figure 2 the visual results on the numerical phantom show the approach works also nicely under noisy conditions and that the exponential length bias correction is reasonable. Quantitative experiments show that it leads to a robust connectivity measure. Compared to [4] the new approach shows smaller connectivity values for bending configurations, which is due to the bending penalty which is inherent to the new approach (see Figure 3). One can also see that the robustness of our approach does not really depend too much on the discretization granularity. Compared to [4] it is in most cases higher (lower standard deviation over the trials). For stronger noise ( $\sigma_{nz} = 0.2$ ) our approach gives relatively higher c-values to false connections, but the c-values itself are more stable. Another difference to [4] is the way the curvature is controlled. If we want for our approach a higher connectivity for bending fibers (ROIs (5,6)), then we also get higher c-values for (1,3) and (2,4). For [4] it is different, the step directions are always back projected onto the nearest most likely fiber direction, which results in higher c-values for the bending (5,6).

To investigate the new approach in-vivo, we considered a group of volunteers which were all scanned twice. We did a ROI-based approach based on the AAL-atlas. Overall, the CMs obtained from our approach and the reference are similar. As one might expect, with our approach strong bending fibers (like the connection between 'Occipital Sup L' to 'Occipital Sup R') are assigned smaller connectivity values. Analysis of the intraclass correlations of c-values shows that the new approach is quite robust. Usually higher angular diffusion  $\sigma_n$  gives more robust c-values. Robustness is further increased by a length bias correction, either linear or exponentially. Compared to [4] our approach shows good performance. For [4] increasing angular diffusion does not help so much. One can see that in regions with low connectivity [4] has problems (see Figure 4f,g)), which goes inline with our finding in the numerical phantom. We found [4] to work best for  $\Delta s = 1$ ,  $\sigma = 0.2$ , revisits are allowed and with length bias correction (see Table I). In this setting the median ICC is 0.68 which is acceptable, 50% of the c-values have a ICC higher than 0.68. The highest value we can achieve with our approach is a median of 0.78. The agreement scores obtained from thresholded c-values show a similar but more pronounced picture (see Figure 4j)). From Figure 5 it can also be seen that the estimated path trail images are meaningful and follow the expected pattern.

## APPENDIX

### A. Operator Formalism

The space of square integrable function on  $\mathbb{R}^n$  is a Hilbert space  $H$  with the inner-product

$$\langle q|p \rangle = \int_{\mathbb{R}^n} q^*(\mathbf{x})p(\mathbf{x})d\mathbf{x}$$

Sometimes we adopt Dirac's bra-ket notation, i.e. by  $|p\rangle$  we denote a vector in  $H$ , by  $\langle p|$  a linear 1-form. The adjoint of a linear operator  $\mathcal{A}$  is defined to be the operator  $\mathcal{A}^+$  such that  $\langle q|\mathcal{A}p \rangle = \langle \mathcal{A}^+q|p \rangle$  for all functions  $q, p \in H$ .

### B. Discretization

Let  $m(\mathbf{r})$  some predefined white matter mask. For each direction  $\mathbf{n}_i$  on the sphere, we create a voxel grid  $\mathbf{r}_{(x,y,z)}^i$  such that the  $x$ -axis is aligned with direction  $\mathbf{n}_i$ . Only valid triples  $(x, y, z) \in \mathbb{N}^3$  are considered where  $m(\mathbf{r}_{(x,y,z)}^i)$  is on. The voxel spacing  $h = |\mathbf{r}_{(x+1,y,z)}^i - \mathbf{r}_{(x,y,z)}^i|$  can be chosen arbitrarily. In the experiments we used  $h = 2mm$  which is resolution of the DTI scan, and  $h = 1mm$ , that is an oversampling factor of 2. The sphere has a natural neighborhood system  $\mathcal{N}(i)$  obtained by Voronoi tessellation. Let  $p_{i,x,y,z}$  be some function on the introduced discrete domain. To discretize the spherical Laplace-Beltrami  $\Delta_n$  operator we define the discrete operator  $\tilde{\Delta}_n$  as

$$(\tilde{\Delta}_n p)_{i,x,y,z} = \sum_{k \in \mathcal{N}(i)} \left( p_{i,x,y,z} - \sum_{\substack{(a,b,c) \in \\ \mathcal{T}(\mathbf{r}_{(x,y,z)}^k)}} w_{k,a,b,c} p_{k,a,b,c} \right)$$

where  $\mathcal{T}(\mathbf{r}_{(x,y,z)}^k)$  is neighborhood system needed for trilinear interpolation at position  $\mathbf{r}_{(x,y,z)}^k$  in the  $k$ -th volume, and  $w_{k,a,b,c}$  are the corresponding weights. However, the matrix  $\tilde{\Delta}_n$  is not symmetric in the sense of the matrix transpose due to the one-sided interpolation. So the final discretized spherical Laplacian is  $\frac{\sigma_n^2}{2A}(\tilde{\Delta}_n + \tilde{\Delta}_n^T)$ . The factor  $A$  is empirically determined to get standard deviations of approximately  $\sigma_n$ .

To implement the convection part, the speed function  $f(\mathbf{r}, \mathbf{n})$  given in the native DTI frame is also transferred by trilinear interpolation onto the new coordinate frame  $f_{i,x,y,z} = f(\mathbf{r}_{(x,y,z)}^i, \mathbf{n}_i)$ . The simulation domain is determined by thresholding  $f_{i,x,y,z}$ . For the convection operator we have to distinguish between 'real' boundaries and boundaries coming from the thresholding. The discretized convection generator  $\tilde{\nabla}$  is defined as

$$-(\tilde{\nabla} p)_{i,x,y,z} = \begin{cases} \frac{p_{i,x-1,y,z} - p_{i,x,y,z}}{h} & \text{otherwise} \\ p_{i,x-1,y,z}/h & \text{if } b_{i,x+1,y,z} = 1 \\ -p_{i,x,y,z}/h & \text{if } b_{i,x-1,y,z} = -1 \\ -p_{i,x,y,z}/h & \text{if } b_{i,x-1,y,z} = 1 \end{cases}$$

where  $b_{i,x,y,z}$  is an boundary indicator, where  $b = 1$  means the boundary is coming from thresholding and  $b = -1$  from a 'real' boundary. Finally, the convection part of the equation is  $-(F\tilde{\nabla} + \tilde{\nabla}F)$ , where  $F$  is the matrix with  $f_{i,x,y,z}$  on the diagonal.

### C. Reference Method

For comparison we followed [4]. Suppose for some given fiber directions, which are always extracted in the same way as for our approach. The state of a walker is its current position  $\mathbf{r}$  and its last step direction  $\mathbf{n}$ . The propagation law for a single walker is: The current voxel contains a set of fiber directions  $\mathbf{d}_i$ . Determine the fiber direction  $\mathbf{d}$  which is closest to the current  $\mathbf{n}$ . If the angle between those is above a threshold of  $80^\circ$  tracking is stopped. Otherwise, disturb this fiber direction by Gaussian noise  $\mathbf{d}_n = \mathbf{d} + \eta_\sigma$  with deviation  $\sigma$ . Renormalize  $\mathbf{d}_n$  to unity and track along this direction with step width  $\Delta s$ , i.e.  $\mathbf{r}^{\text{new}} = \mathbf{r} + \Delta s \mathbf{d}_n$  and set  $\mathbf{n}^{\text{new}} = \mathbf{d}_n$ . If the new position is out of the tracking mask, stop tracking. If desired, one can also stop tracking whenever a voxel is visited more than once. During tracking we count how often a walker has visited a voxel resulting in a probabilistic map (PM). Alternatively, to account for the length bias, one can also weight with visitation count by the mean length of all walkers visited the voxel. To compute the connectivity value between ROI A and ROI B,  $N$  walkers are ejected in each voxel in ROI A. The connectivity value is then the sum over the PM in ROI B. To get a symmetric value the connectivity from A to B is averaged with the connectivity from B to A. To set  $N$  we computed the intra-scan ICC, i.e. for each subject and scan in the group we started the algorithm twice and computed the ICC between the two algorithm runs. We set  $N$ , such that the median ICC over all ROI pairs is above 0.95, which resulted in  $N = 5000$  per voxel.

### REFERENCES

- [1] Lars Andersson and Bruce K Driver. Finite dimensional approximations to wiener measure and path integral formulas on manifolds. *Journal of functional analysis*, 165(2):430–498, 1999.
- [2] P. J. Basser, S. Pajevic, C. Pierpaoli, J. Duda, and A. Aldroubi. In vivo fiber tractography using DT-MRI data. *Magn Reson Med*, 44(4):625–32, 2000. 20481737 0740-3194 Journal Article.
- [3] PG Batchelor, DLG Hill, D Atkinson, F Calamante, and A Connelly. Fibre-tracking by solving the diffusion-convection equation. In *Proc. ISMRM*, volume 10, 2002.
- [4] T. E. J. Behrens, H. J. Berg, S. Jbabdi, M. F. S. Rushworth, and M. W. Woolrich. Probabilistic diffusion tractography with multiple fibre orientations: What can we gain? *Neuroimage*, 34(1):144–155, 2007. English Article 1053-8119.
- [5] Mats Björnemo, Anders Brun, Ron Kikinis, and Carl-Fredrik Westin. Regularized stochastic white matter tractography using diffusion tensor mri. In *Medical Image Computing and Computer-Assisted Intervention—MICCAI 2002*, pages 435–442. Springer, 2002.
- [6] M Chaichian and A Demichev. Path integrals in physics, vol. 1: Stochastic processes and quantum mechanics. *Bristol, UK: IOP*, 2001.
- [7] Detlef Dürr and Alexander Bach. The onsager-machlup function as lagrangian for the most probable path of a diffusion process. *Communications in Mathematical Physics*, 60(2):153–170, 1978.
- [8] Richard P Feynman and Albert R Hibbs. *Quantum mechanics and path integrals: Emended edition*. Courier Dover Publications, 2012.
- [9] Ola Friman, Gunnar Farneback, and C-F Westin. A bayesian approach for stochastic white matter tractography. *Medical Imaging, IEEE Transactions on*, 25(8):965–978, 2006.
- [10] Karl J. Friston, John T. Ashburner, Stefan J. Kiebel, Thomas E. Nichols, and William D. Penny, editors. *Statistical Parametric Mapping: The Analysis of Functional Brain Images*. Elsevier, 2007.
- [11] L Garrido, D Lurié, and M San Miguel. Stochastic quantization and detailed balance in fokker-planck dynamics. *Journal of Statistical Physics*, 21(3):313–335, 1979.
- [12] Nathan S Hageman, Arthur W Toga, Katherine L Narr, and David W Shattuck. A diffusion tensor imaging tractography algorithm based on navier-stokes fluid mechanics. *Medical Imaging, IEEE Transactions on*, 28(3):348–360, 2009.
- [13] P. Hagmann, J. P. Thiran, L. Jonasson, P. Vanderghenst, S. Clarke, P. Maeder, and R. Meuli. Dti mapping of human brain connectivity: statistical fibre tracking and virtual dissection. *Neuroimage*, 19(3):545–554, 2003. English 1053-8119.
- [14] H Haken. Generalized onsager-machlup function and classes of path integral solutions of the fokker-planck equation and the master equation. *Zeitschrift für Physik B Condensed Matter*, 24(3):321–326, 1976.
- [15] Hidemi Ito. A characterization of the detailed balance from a viewpoint of the onsager-machlup theory. *Progress of Theoretical Physics*, 66(2):454–460, 1981.
- [16] Derek K Jones, editor. *Diffusion MRI: Theory, Methods and Applications*. Oxford University Press, 2010.
- [17] Mark Kac. On distributions of certain wiener functionals. *Trans. Amer. Math. Soc.*, 65:1–13, 1949.
- [18] Hagen Kleinert. *Path integrals in quantum mechanics, statistics, polymer physics, and financial markets*. World Scientific, 2009.
- [19] J. Mangin. A framework based on spin glass models for the inference of anatomical connectivity from diffusion-weighted mr data - a technical review. *NMR Biomed*, 15(7-8):481–492, 2002.
- [20] O. Michailovich. Spatially regularized compressed sensing for high angular resolution diffusion imaging. *IEEE Transactions on Medical Imaging*, 30:1100–1115, 2011.
- [21] S. Mori, B. J. Crain, V. P. Chacko, and P. C. van Zijl. Three-dimensional tracking of axonal projections in the brain by magnetic resonance imaging. *Ann Neurol*, 45(2):265–9, 1999. 99142739 0364-5134 Journal Article.
- [22] G. J. M. Parker, H. A. Haroon, and C. A. M. Wheeler-Kingshott. A framework for a streamline-based probabilistic index of connectivity (pico) using a structural interpretation of mri diffusion measurements. *J Magn Reson Imaging*, 18(2):242–254, 2003. English 1053-1807.
- [23] M. Reisert and V. Kiselev. Fiber continuity: An anisotropic prior for odg estimation. *IEEE Trans Med Imaging*, 30(6):1274–1283, June 2011.
- [24] M. Reisert, I. Mader, C. Anastasopoulos, M. Weigel, S. Schnell, and V. Kiselev. Global fiber reconstruction becomes practical. *Neuroimage*, 54(2):955–62, 2011.
- [25] M. Reisert, H. Skibbe, and V. Kiselev. Fiber density estimation by tensor divergence. *Medical Image Computing and Computer-Assisted Intervention—MICCAI 2012*, pages 297–304, 2012.
- [26] Youcef Saad and Martin H Schultz. Gmres: A generalized minimal residual algorithm for solving nonsymmetric linear systems. *SIAM Journal on scientific and statistical computing*, 7(3):856–869, 1986.
- [27] J Tournier, Fernando Calamante, David G Gadian, Alan Connelly, et al. Diffusion-weighted magnetic resonance imaging fibre tracking using a front evolution algorithm. *NeuroImage*, 20(1):276–288, 2003.
- [28] J.D. Tournier, F. Calamante, D.G. Gadian, and A. Connelly. Robust determination of the fibre orientation distribution in diffusion mri: Non-negativity constrained super-resolved spherical deconvolution. *NeuroImage*, 35(4):1459–1472, 2007.
- [29] David S Tuch, John W Belliveau, and Van J Wedeen. A path integral approach to white matter tractography. In *Proceedings of the 8th Annual Meeting of ISMRM, Denver*, page 791, 2000.
- [30] Nathalie Tzourio-Mazoyer, Brigitte Landeau, Dimitri Papanathanassiou, Fabrice Crivello, Olivier Etard, Nicolas Delcroix, Bernard Mazoyer, and Marc Joliot. Automated anatomical labeling of activations in spm using a macroscopic anatomical parcellation of the mni mri single-subject brain. *Neuroimage*, 15(1):273–289, 2002.
- [31] Nicolaas Godfried Van Kampen. *Stochastic processes in physics and chemistry*, volume 1. Elsevier, 1992.
- [32] Myron Zhang, Ken E Sakaie, and Stephen E Jones. Logical foundations and fast implementation of probabilistic tractography. *Medical Imaging, IEEE Transactions on*, 2013.